

Short Communication

## B, N dual-doped Graphene/Au@Pt Nanomaterials as Sensor for Determination of Aflatoxin B<sub>1</sub>

Shaoping Feng<sup>1,2</sup>, Jinming Meng<sup>1,2</sup>, Jinming Guo<sup>1,2</sup>, Xianlan Chen<sup>1,2,\*</sup>, Guowei Zhang<sup>1,2,\*</sup>, Wei Liu<sup>1,2,\*</sup>, Guiyang Liu<sup>1,2</sup>, Guangming Yang<sup>1,2</sup>, Hongyan Sun<sup>1,2</sup>

<sup>1</sup> College of Science, Honghe University, Mengzi, 661199, Yunnan, P.R.China

<sup>2</sup> Local Characteristic Resource Utilization and New Materials Key Laboratory of Universities in Yunnan, Honghe University, Mengzi, 661199, Yunnan, China

\*E-mail: [13489086418@163.com](mailto:13489086418@163.com), [yunnmzh@126.com](mailto:yunnmzh@126.com), [liuwei4728@126.com](mailto:liuwei4728@126.com)

Received: 16 April 2020 / Accepted: 31 May 2020 / Published: 10 July 2020

In this study, B, N dual-doped graphene/Au@Pt nanomaterials (BN-G/Au@Pt NRs) was prepared by high pressure hydrothermal approach with the mass ratios of graphemes oxide (GO), urea (CH<sub>4</sub>N<sub>2</sub>O) and B<sub>2</sub>O<sub>3</sub> were 1:25:30. BN-G/Au@Pt NRs have plenty of monolayer nanosheets with large-area and maintain the characteristic three dimension porous structure of grapheme. More importantly, the as-synthesized BN-G/Au@Pt NRs present advantageous biocompatibility and multivalent affinity interactions with anti-AFB<sub>1</sub>, which can amplify immunoreactions. Therefore, the designed immunosensor of BN-G/Au@Pt NRs/anti-AFB<sub>1</sub>/BSA/AFB<sub>1</sub>/GCE can be used to determinate AFB<sub>1</sub> under optimal condition and exhibit excellent sensitivity with a wide linear range from 0.025 ng·mL<sup>-1</sup> to 25.00 ng·mL<sup>-1</sup> and low the detection limits of 0.017 ng·mL<sup>-1</sup>. Moreover, the designed BN-G/Au@Pt NRs/anti-AFB<sub>1</sub>/BSA/AFB<sub>1</sub>/GCE immunosensor was successfully applied for AFB<sub>1</sub> determination in rice samples with acceptable recovery range of 98.0-101.1 %, which demonstrated that the proposed method could be a suitable candidate for AFB<sub>1</sub> detection in food industries.

**Keywords:** Aflatoxin B<sub>1</sub>; B, N dual-doped grapheme (BN-G); BS-G/Au@Pt NRs; Electrochemical immunosensor

### 1. INTRODUCTION

Aflatoxins, as an important member of mycotoxins, belong to the fungal metabolites and have been found in human diets such as grains, various fruits and nuts [1, 2]. Aflatoxins are oxygenated chemicals with high toxicity, and cause disease in man or animals such as carcinogenesis, teratogenicity, mutagenicity and immunosuppressive activity [3, 4]. So far there are more than 20 aflatoxins with high toxicity have been identified, among which aflatoxin B<sub>1</sub> (AFB<sub>1</sub>) present the highest potential toxicity [5, 6]. Therefore, developing a specific, convenient and sensitive method for

determination of AFB<sub>1</sub> is necessary and desirable due to its low concentration in food products and high toxicity.

Various analytical methods including TLC [7], LC-MS/MS [8], ELISA [9], HPLC [10, 11], have been proposed for detection of AFB<sub>1</sub>. However, these methods have suffered from several disadvantages, such as time consuming, high-cost and complex sample processing and expensive instruments [12]. Nowadays, several electrochemical sensors with high selectivity have been developed for detection of AFB<sub>1</sub> and attracted special attention [13]. For examples, Gevaerd et al. constructed a novel electrochemical sensor of NPAuGQD-SPE and employed for detection of AFB<sub>1</sub> in malted barley with a wide linear range (1.0-50.0 nM) and low detection limit (0.47 nM) [14]. Banitaba et al. successfully constructed IL-CPEs sensor and used to determinate of AFB<sub>1</sub> with the linear range and detection limit of  $8.0 \times 10^{-8}$ - $5.91 \times 10^{-7}$  M and  $2.0 \times 10^{-8}$  M, respectively [15]. Li et al. reported Ab-SGIL-GCE electrode and used for determination of AFB<sub>1</sub> in bee pollen, and the linear range and detection limit are 0.1-10 ng·mL<sup>-1</sup> and 0.01 ng·mL<sup>-1</sup> respectively [13].

In order to develop an efficient, convenient and fast method with high sensitivity for determination of AFB<sub>1</sub> in food products, B, N dual-doped graphene/Au@Pt nanomaterials modified electrode (BN-G/Au@Pt NRs/GCE) was developed in this study. The established electrochemical sensor was sensitive and reliable for determination of AFB<sub>1</sub> in rice samples with excellent stability and high accuracy.

## 2. EXPERIMENTAL

### 2.1 Reagents

Aflatoxin B<sub>1</sub> (AFB<sub>1</sub>), albumin from bovine serum (BSA $\geq$ 98%), monoclonal anti-AFB<sub>1</sub> antibody (anti-AFB<sub>1</sub>), urea (AR, CH<sub>4</sub>N<sub>2</sub>O), HAuCl<sub>4</sub>·3H<sub>2</sub>O (AR,  $\geq$ 99.99%) and H<sub>2</sub>PtCl<sub>6</sub> (AR,  $\geq$ 99.8) were purchased from Sinopharm Chemical Reagent Co. Ltd. (Shanghai, China). Graphite (99.95%, 325 mesh) powder and B<sub>2</sub>O<sub>3</sub> (AR,  $\geq$ 99%) were purchased from Alfa Aesar Co. Ltd. (Tianjin, China). Phosphate buffer solution (PBS, 0.10 M NaH<sub>2</sub>PO<sub>4</sub>-Na<sub>2</sub>HPO<sub>4</sub>) was used to adjust the pH of solution. All other chemicals used were of analytical reagent grade.

### 2.2 Instruments and characterizations

X-ray diffraction (XRD, X'pert, Philips, Holland) and XPS (Thermal Scientific K-Alpha XPS spectrometer) were employed to investigate the crystalline structures and elemental compositions of the BN-G/Au@Pt NRs. The surface morphologies and microstructure of BN-G/Au@Pt NRs were characterized by SEM (Nova Nano SEM 230, FEI, USA) and HRTEM (Tecnai G2 F20 S-TWIN, 200 kV, FEI Company, USA).

The electrochemical workstation (CHI 660C, Shanghai) was used to obtain the cyclic voltammetry (CV) and differential pulse voltammogram (DPV). The electrochemical cell consisted of a three electrode system with a bare glassy carbon electrode (GCE, 3.0 mm in diameter) or modified

working electrode as a working electrode, a platinum wire as a counter electrode and Ag/AgCl electrode as a reference electrode. The mixed solution of 10.00 mM  $[\text{Fe}(\text{CN})_6]^{3-/4-}$ , 0.10 M KCl and PBS (pH=7.0, 0.10 M  $\text{NaH}_2\text{PO}_4\text{-Na}_2\text{HPO}_4$ ) were added into the electrochemical cell and all the determination solutions were purged with  $\text{N}_2$  for at least 15.0 min before measurements. All measurements were carried out at room temperature (25 °C).

### 2.3 Preparation of BN-G/Au@Pt NRs

In order to prepare BN-G/Au@Pt NRs, 0.5 mg/mL GO with uniform dispersion was firstly obtained by sonication for a certain time. The as-prepared GO (0.5 mg/L), melamine ( $\text{C}_3\text{H}_6\text{N}_6$ ) and  $\text{B}_2\text{O}_3$  were mixed with a mass ratio of 1:25:30, followed by the addition  $\text{HAuCl}_4$  (300  $\mu\text{L}$  50 mM) and  $\text{H}_2\text{PtCl}_6$  (375  $\mu\text{L}$  40 mM) and sonicated for 30 min. The solution was transferred to a high-pressure reaction kettle and heated at 160 °C for 7 h under stirring. Then, the obtained mixture was centrifuged and washed 3~5 times until the excess urea ( $\text{CH}_4\text{N}_2\text{O}$ ) and  $\text{B}_2\text{O}_3$  were eluted.

### 2.4 Fabrication of the immunosensor

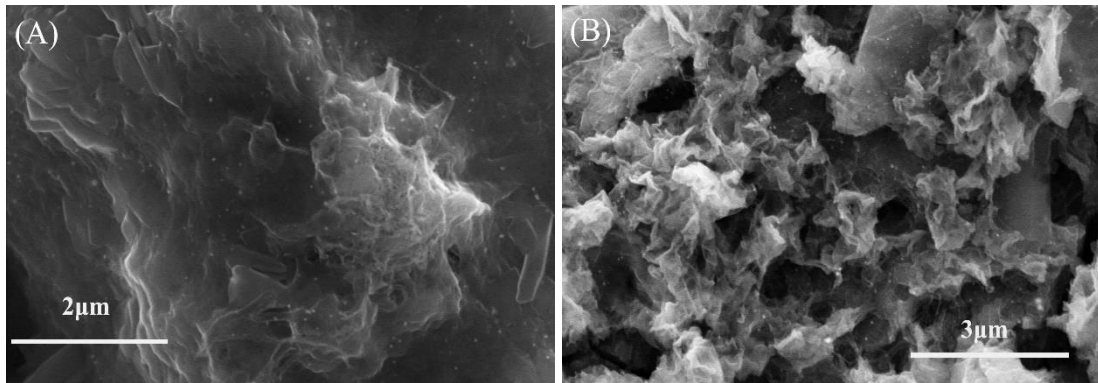
The fabrication procedure of the modified glassy carbon electrode (GCE), including polishing, ultrasonication and drying, were as same as in our previous works [16]. After activation, 15  $\mu\text{L}$  BN-G/Au@Pt NRs was uniformly dropped on the surface of the modified GCE and evaporated the solvent to prepare BN-G/Au@Pt NRs/GCE. Then, 10  $\mu\text{L}$  150  $\mu\text{g/mL}$  anti-AFB<sub>1</sub> were pipetted over the BN-G/Au@Pt NRs/GCE and incubated at 37.0 °C for 40.0 min, followed by rinsing with blank PBS (pH= 7.0, 0.10 M  $\text{NaH}_2\text{PO}_4\text{-Na}_2\text{HPO}_4$ ) to remove the residual anti-AFB<sub>1</sub> and drying at 25 °C, formed modified electrode was recorded as BN-G/Au@Pt NRs/anti-AFB<sub>1</sub>/GCE. Further, the non-specific sites of BN-G/Au@Pt NRs/anti-AFB<sub>1</sub>/GCE was blocked with BSA (10.0 mL, 2.0 wt.%) and kept at 37.0 °C for 40.0 min to prepare BN-G/Au@Pt NRs /anti-AFB<sub>1</sub>/BSA/GCE. Finally, the obtained BN-G/Au@Pt NRs /anti-AFB<sub>1</sub>/BSA/GCE was incubated at 37.0 °C for 30.0 min with 10  $\mu\text{L}$  10 ng/mL AFB<sub>1</sub> and washed with blank PBS (pH= 7.0, 0.10 M  $\text{NaH}_2\text{PO}_4\text{-Na}_2\text{HPO}_4$ ) until to remove residual AFB<sub>1</sub>, and the BN-G/Au@Pt NRs /anti-AFB<sub>1</sub>/BSA/AFB<sub>1</sub>/GCE was obtained after drying.

### 2.5 Sample preparation

1.00 g pulverized rice sample and certain AFB<sub>1</sub> were uniformly mixed and extracted for 45.0 min with 5.0 mL methanol-water (80:20, v/v). The obtained mixture was centrifuged at 10000.0 rpm for 15.0 min and diluted into different concentration with PBS (pH= 7.0, 0.10 M  $\text{NaH}_2\text{PO}_4\text{-Na}_2\text{HPO}_4$ ) for determination. The samples were stored at -20.0 °C before measurement. The AFB<sub>1</sub> spiked rice was incubated for 50.0 min, and then washed in PBS (pH= 7.0, 0.10 M  $\text{NaH}_2\text{PO}_4\text{-Na}_2\text{HPO}_4$ ) and dried under  $\text{N}_2$  followed by electrochemical measurements.

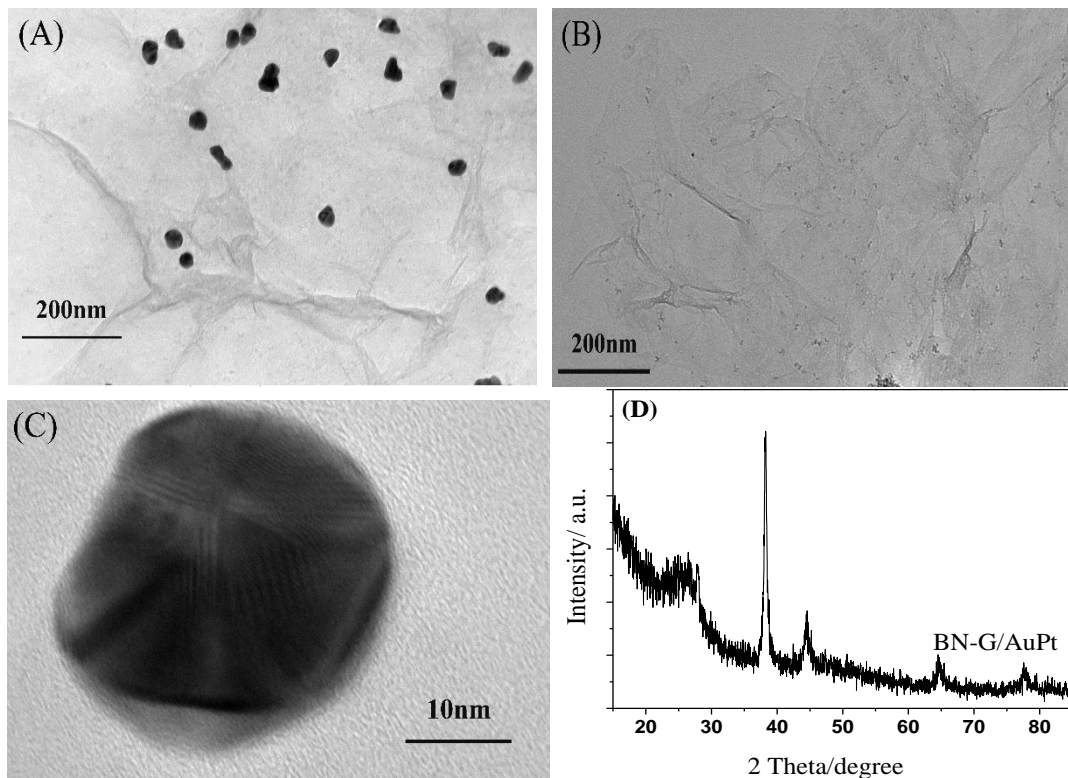
### 3. RESULTS AND DISCUSSION

#### 3.1 Characterization of BN-G/Au@Pt NRs



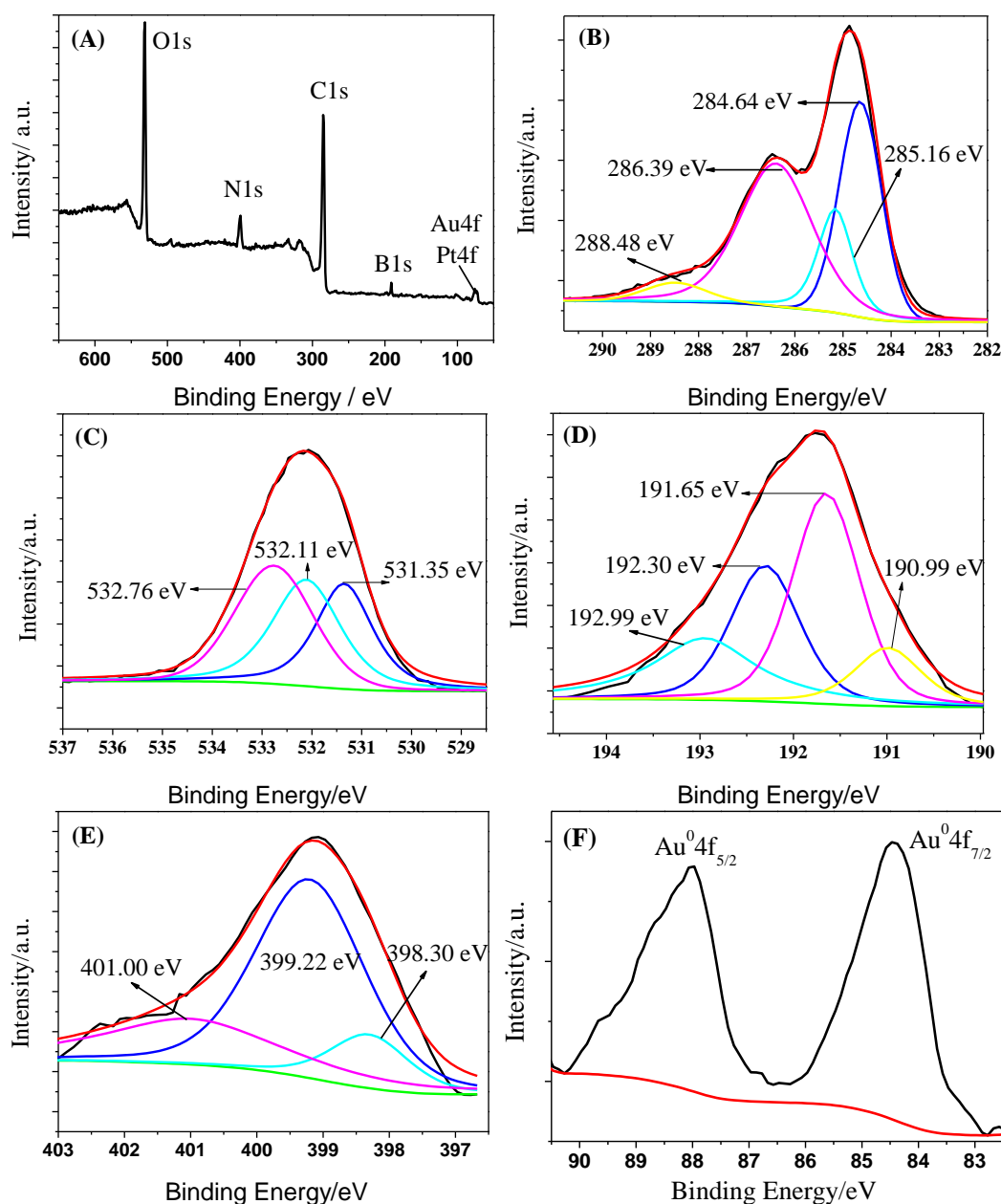
**Figure 1.** SEM of BN-G/Au@Pt NRs

SEM images of BN-G/Au@Pt NRs showed that numerous Au@Pt NRs have uniformly anchored on BN-G nanosheets with sheet-like and folded structure (Fig. 1(A) and Fig. 1(B)). It is clear observed that BN-G/Au@Pt NRs still maintain the characteristic three dimension porous structure of grapheme, and there are plenty of monolayer nanosheets with large-area, which resulted in excellent electrolyte penetration and intrinsic property.



**Figure 2.** TEM of BN-G/Au@Pt NRs (A-C), XRD of BN-G/Au@Pt NRs (D)

TEM with different magnification investigated the structure and morphology of BN-G/Au@Pt NRs in Fig. 2 (A), Fig. 2 (B) and Fig. 2 (C). From Fig. 2 (A), Au@Pt NRs are uniformly distributed on the transparent BN-G sheets and there are almost no free Au@Pt NRs, indicating that numerous Au@Pt NPs have uniformly anchored on the surface of BN-G. In Fig. 2 (B) and Fig. 2 (C), the BN-G/Au@Pt NR showed spherical particle morphology with an estimated diameter of 32 nm and present crumpled or wrinkled sheets. XRD has been employed for the phase composition of BN-G/Au@Pt NRs in Fig. 2 (D). There is an obvious peak at  $2\theta = 24.44^\circ$ , which is attributed to the (002) plane of graphene sheets [16]. In addition, the (111), (200), (220) and (311) planes of BN-G/Au@Pt NRs exhibited four distinguishable peaks at  $38.26^\circ$ ,  $44.56^\circ$ ,  $64.52^\circ$  and  $77.58^\circ$  of  $2\theta$  values, respectively, which are corresponding to both Au and Pt diffractions [17, 18]. These results indicated that BN-G/Au@Pt NRs have been synthesized successfully.



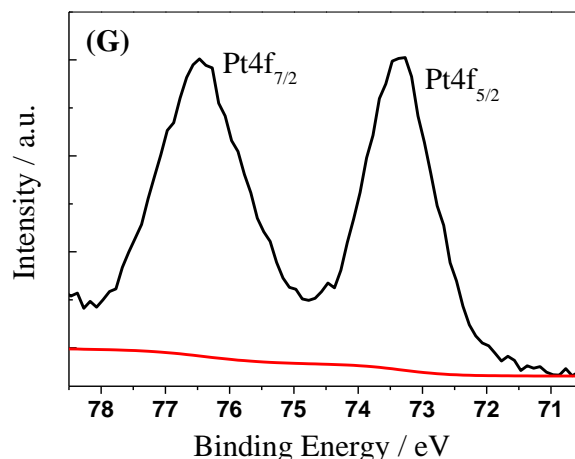


**Figure 3.** (A) Full-scan XPS of BN-G/Au@Pt NRs(A), (B-F) high resolution C1s, O1s, B1s,N1s, Au 4f and Pt 4f XPS scan of BN-G/Au@Pt NRs

In order to ascertain the element components of BN-G/Au@Pt NRs, XPS was employed and the results were shown in Fig. 3. Four distinguishable peaks at 531.17eV (O1s), 399.17 eV (N1s), 285.17 eV (C1s), 191.17 eV (B1s) were observed in Fig. 3(A), demonstrating that the B and N atoms have been completely bonded to carbon atoms [16, 19]. Four fitting peaks of 284.64 eV (C=C), 285.16 eV (C-C and C-N), 286.39 eV (C-O) and 288.48 eV (-COOH) were obtained in Fig. 3(B) [20]. In addition, XPS spectra of O1s was shown in Fig. 3(C), there are three peaks at 531.35 eV (C=O-OH), 532.11 eV (C=O) and 532.76 eV (C-OH) [20]. From Fig. 3(D), four fitting peaks of 190.99 eV, 191.65 eV, 192.30 eV and 192.99 eV were attributed to B-C, BCO<sub>2</sub>, BC<sub>2</sub> and B-O bands, indicating that B atom has embedded in the grapheme sheet [16, 21]. Three peaks at 398.30 eV (pyridinic N), 399.22 eV (yrrolic N) and 401.00 eV (graphitic N) were found in XPS spectra of N1s (Fig. 3(E)) [22]. Fig. 3(F) exhibits the binding energies Au 4f<sub>7/2</sub> (84.47eV) and Au 4f<sub>5/2</sub> (87.97eV) in BN-G/Au@Pt NRs [23]. In Fig. 3(G), there are two characteristic peaks at 73.27 eV and 76.47 eV corresponding to Pt 4f<sub>7/2</sub> and Pt 4f<sub>5/2</sub>, respectively [24, 25].

### 3.2. Electrochemical characterization of BN-G/Au@Pt NRs

To characterize the interfacial properties of the immunosensor, the properties of modified electrodes, including BN-G/Au@Pt NRs/GCE (a), BN-G/Au@Pt NRs/anti-AFB<sub>1</sub>/GCE (b), BN-G/Au@Pt NRs/anti-AFB<sub>1</sub>/BSA/GCE (c) and BN-G/Au@Pt NRs/anti-AFB<sub>1</sub>/BSA/AFB<sub>1</sub>/GCE (d), were investigated by CV measurement in Fig. 4. Obviously, it is the BN-G/Au@Pt NRs/GCE (a) that has the highest peak current ( $I_p$ ), while a clearly decrease of  $I_p$  was observed after immobilization of anti-AFB<sub>1</sub> (BN-G/Au@Pt NRs/anti-AFB<sub>1</sub>/GCE (b)). These results indicated that the as-prepared BN-G/Au@Pt NRs possess large effective surface area and excellent electron-transfer abilities. In addition,  $I_p$  decreased slightly with the immobilization of BSA (BN-G/Au@Pt NRs/anti-AFB<sub>1</sub>/BSA/GCE (c)), suggesting that active sites at the modified electrode which caused nonspecific adsorption were blocked partially. After incubation with 10.00 ng·mL<sup>-1</sup> AFB<sub>1</sub>,  $I_p$  exhibits an obvious decrease, which presumably reason was that the inert property of protein and the generation of antibody-antigen

immunocomplexes result in the decreased ferricyanide diffusion ability. These results above demonstrated that the immobilized electrode was constructed successfully. More importantly, the highly oriented immobilization of AFB<sub>1</sub> could be modified onto the electrode due to the special active area of the as-prepared BN-G/Au@Pt NRs.

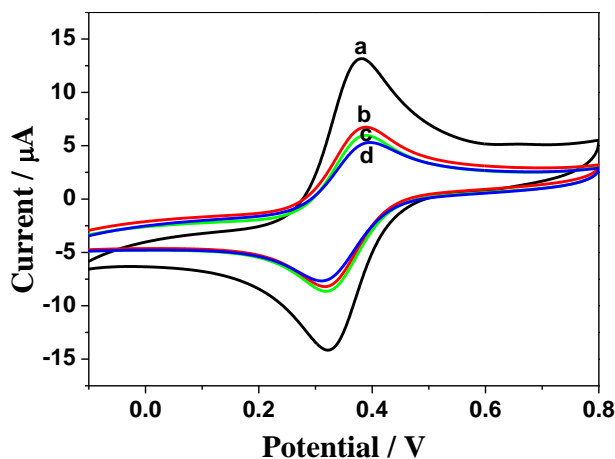


**Figure 4.** CVs of BN-G/Au@Pt NRs/GCE (a), BN-G/Au@Pt NRs/anti-AFB<sub>1</sub>/GCE (b), BN-G/Au@Pt NRs/anti-AFB<sub>1</sub>/BSA/GCE (c) and BN-G/Au@Pt NRs/anti-AFB<sub>1</sub>/BSA/AFB<sub>1</sub>/GCE (d). The measurements were carried out in N<sub>2</sub>-saturated 1.00 mM K<sub>3</sub>[Fe(CN)<sub>6</sub>] and 0.50 M KCl mixture solution at 50.0 mV/s. The concentration of anti-AFB<sub>1</sub> and AFB<sub>1</sub> are 100.00 μg·mL<sup>-1</sup> and 10.00 ng·mL<sup>-1</sup>, respectively.

### 3.3 Determination of optimized conditions for immunoassay of AFB<sub>1</sub>

The effects of pH of PBS, the concentration of anti-AFB<sub>1</sub>, the immobilization time of anti-AFB<sub>1</sub>, and the incubation time between antibody and antigen on the determination of 10.00 ng·mL<sup>-1</sup> AFB<sub>1</sub> have been investigated in Fig. 5. The electrochemical responses of 10.00 ng·mL<sup>-1</sup> AFB<sub>1</sub> on BN-G/Au@Pt NRs /anti-AFB<sub>1</sub>/BSA/AFB<sub>1</sub>/GCE with different pH values (5.5, 6.0, 6.5, 7.0, 7.5) at 50 mV/s were investigated and shown in Fig. 5(A). The I<sub>p</sub> reached to the minimum when pH value reached to 7.0, demonstrating that pH 7.0 was the suitable pH for determination of AFB<sub>1</sub> and used in further experiments. As shown in Fig. 5(B), the I<sub>p</sub> decreased with the concentration of immobilized anti-AFB<sub>1</sub> increased at the beginning (< 150 mg·mL<sup>-1</sup>), and then decreased obviously. Thus, 150 mg·mL<sup>-1</sup> of anti-AFB<sub>1</sub> concentration was a suitable optimum. In Fig. 5(B), DPV response of AFB<sub>1</sub> decreased steeply with the increasing of incubation time before 50.0 min and then increased obviously, indicating that 50.0 min was chosen as an optional assembly time of anti-AFB<sub>1</sub>. Furthermore, 40.0 min of immobilization time of AFB<sub>1</sub> was selected for AFB<sub>1</sub> determination in this study because of the minimum DPV response so as to ensure a sufficient reaction between AFB<sub>1</sub> and the modified electrode.

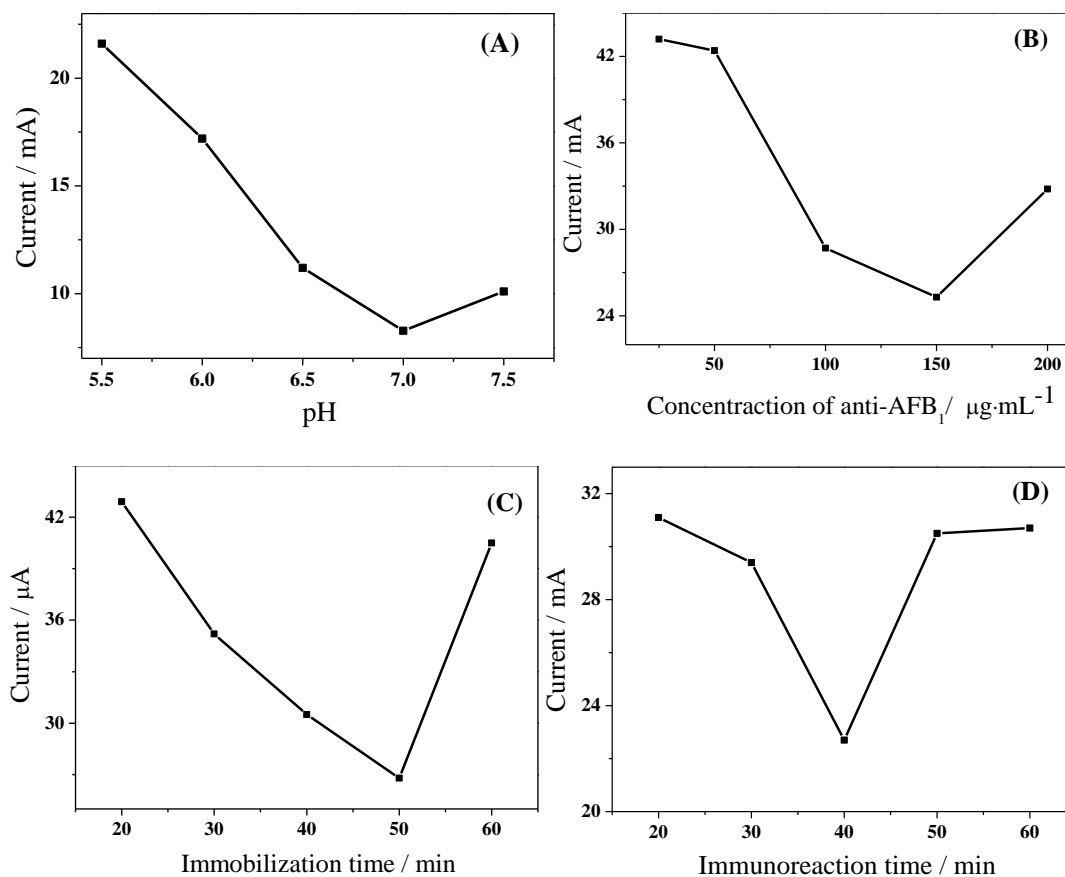


**Figure 5.** Effect of pH of PBS (A), anti-AFB<sub>1</sub> concentration(B), anti-AFB<sub>1</sub> immobilization time(C) and AFB<sub>1</sub> immunoreaction time (D) on  $I_p$  of the immunosensor. The experimental conditions were optimized by recording DPV toward mixed solution of 10.00 ng·mL<sup>-1</sup> AFB<sub>1</sub>, 10.00 mM [Fe(CN)<sub>6</sub>]<sup>3-/4-</sup> and 0.10 M KCl at 50 mV/s vs. Ag/AgCl.

### 3.4 Analytical performance of designed immunosensor

DPV responses at BN-G/Au@Pt NRs/anti-AFB<sub>1</sub>/BSA/AFB<sub>1</sub>/GCE were investigated with different AFB<sub>1</sub> concentration from 0.025~25.00 ng·mL<sup>-1</sup> in Fig. 6(A). A linearly decrease of the  $I_p$  can be observed with the successive increasing of AFB<sub>1</sub> concentrations from 0.025 to 25.00 ng·mL<sup>-1</sup>. From Fig. 6(B), a linear relationship between  $I_p$  and AFB<sub>1</sub> concentrations was found and the regression equation was  $I_p = 26.645 - 0.289c$  (ng·mL<sup>-1</sup>), and the calculated detection limits was 0.017 ng·mL<sup>-1</sup> (S/N=3). These results indicated that the as-synthesized BN-G/Au@Pt NRs present an excellent electrochemical activity and the designed immunosensor can be used to determinate AFB<sub>1</sub> under optical condition, which could be a suitable candidate for AFB<sub>1</sub> detection in food industries. The comparison of similar electrodes and BN-G/Au@Pt NRs/anti-AFB<sub>1</sub>/BSA/AFB<sub>1</sub>/GCE for AFB<sub>1</sub> determination was shown in Table 1.

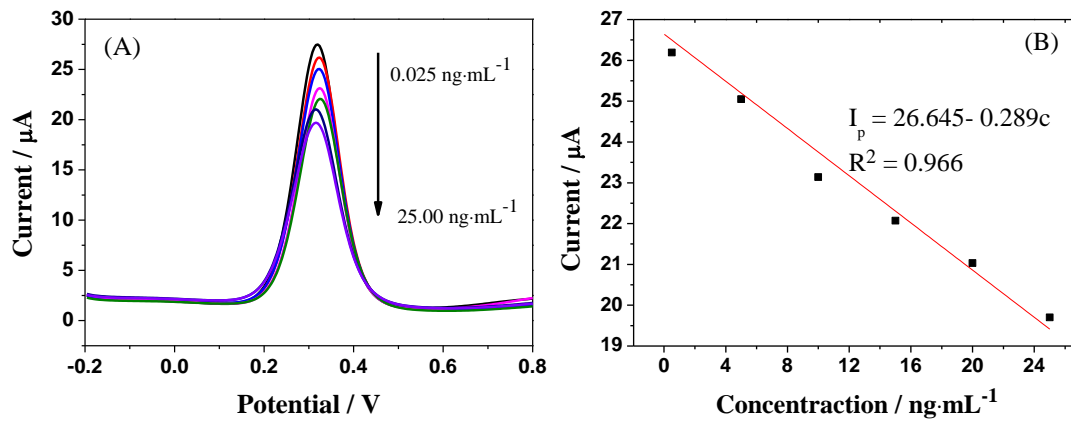


**Figure 6.** (A) DPV at BN-G/Au@Pt NRs/anti-AFB<sub>1</sub>/BSA/AFB<sub>1</sub>/GCE, AFB<sub>1</sub> concentrations: 0.025, 0.05, 5.00, 10.00, 15.00, 20.00, 25.00 ng·mL<sup>-1</sup>. (B) The relationship of I<sub>p</sub> with AFB<sub>1</sub> concentration.

**Table 1.** Comparison of similar electrodes and BN-G/Au@Pt NRs/anti-AFB<sub>1</sub>/BSA/AFB<sub>1</sub>/GCE for AFB<sub>1</sub> determination

Electrodes	Linear range (ng·mL <sup>-1</sup> )	Detection limit (ng·mL <sup>-1</sup> )	Reference
Ab-SGIL-GCE electrode	0.1-10	0.01	[10]
BSA/anti-AFB <sub>1</sub> /AuNPs/CHI/GCE	0.6-110	0.2	[14]
BSA/anti-AFB <sub>1</sub> /CHI-AuNPs/Au microelectrode	0.1-30	0.06	[16]
HRP-anti AFB <sub>1</sub> /AuNPs/TiO <sub>2</sub> /RTIL/Nafion/GCE	0.1-12	0.05	[17]
HRP/anti-AFB <sub>1</sub> /AuNPs/AET/microelectrode	0.5-10	0.1	[18]
BN-G/Au@Pt NRs/anti-AFB <sub>1</sub> /BSA/AFB <sub>1</sub> /GCE	0.025-25	0.017	This work

### 3.5 Analytical application in spiked rice samples

**Table 2.** Results of AFB<sub>1</sub> detection in spiked rice samples (n=3)

Sample	Added (ng·mL <sup>-1</sup> )	Found (ng·mL <sup>-1</sup> )	Recovery (%)
Rice	10.00	9.80	98.0
	50.00	49.80	98.2
	100.00	101.10	101.1

In this study, the AFB<sub>1</sub> concentration in rice samples was determined to further investigate the applicability of the designed BN-G/Au@Pt NRs/anti-AFB<sub>1</sub>/BSA/AFB<sub>1</sub>/GCE immunosensor. We spiked AFB<sub>1</sub> standards (10.00 ng·mL<sup>-1</sup>, 50.00 ng·mL<sup>-1</sup> and 100.00 ng·mL<sup>-1</sup>) into blank rice, followed by a sample preparation procedure (subsection 2.5). The DPV results showed that the recovery was 98.0-101.1 % (Table 2), demonstrating that the proposed method was reasonable for AFB<sub>1</sub> determination in rice samples.

#### 4. CONCLUSIONS

In summary, B, N dual-doped graphene/Au@Pt nanomaterials (BN-G/Au@Pt NRs) with excellent electron-transfer abilities have been developed and used to design immunosensor for AFB<sub>1</sub> determination. In particular, The BN-G/Au@Pt NRs maintain the characteristic three dimension porous structure of grapheme and present large effective surface area, which resulted in excellent electrolyte penetration and intrinsic property. Interestingly, the as-synthesized BN-G/Au@Pt NRs could be immobilization of anti-AFB<sub>1</sub> effectively, and have been prepared to BN-G/Au@Pt NRs/anti-AFB<sub>1</sub>/BSA/AFB<sub>1</sub>/GCE for AFB<sub>1</sub> determination. The designed immunosensor of BN-G/Au@Pt NRs/anti-AFB<sub>1</sub>/BSA/AFB<sub>1</sub>/GCE exhibits excellent sensitivity with a wide linear range (0.025 ng·mL<sup>-1</sup>-25.00 ng·mL<sup>-1</sup>) and low the detection limits (0.017 ng·mL<sup>-1</sup>). Furthermore, the immunosensor was successfully applied to selective determination of AFB<sub>1</sub> in rice samples and the recovery was in the range of 98.0-101.1 %, offering the potential application for detecting of AFB<sub>1</sub> in real samples.

#### ACKNOWLEDGMENTS

The authors gratefully acknowledge the financial support from the Yunnan education department of Scientific Research Foundation (2018JS478, 2019J1183), Yunnan Local Colleges Applied Basic Research Projects (2018FH001-114, 2018FH001-049 and 2017FD157) and the National Natural Science Foundation of China (51362012, 51662007 and 51574213).

#### References

1. A. Sheibani, M. Tabrizchi, H.S. Ghaziaskar, *Talanta*, 75 (2008) 233-238.
2. M. Ventura, A. Gómez, I. Anaya, J. Díaz, F. Broto, M. Agut, L. Comellas, *J. Chromatogr. A*, 1048 (2004) 25-29.
3. F.Y. Yu, A.V. Gribas, M.M. Vdovenko, I.Y. Sakharov, *Talanta*, 107 (2013) 25-29.
4. Á.M. Móricz, Z. Fatér, K.H. Otta, E. Tyihák, E. Mincsovic, *Microchem. J.*, 85 (2007) 140-144.
5. H. Wang, Y.H. Zhang, Y.G. Chu, H.M. Ma, Y. Li, D. Wu, B. Du, Q. Wei, *Talanta*, 147 (2016) 556-560.
6. H.Y. Ge, Y.Y. Jiang, F.Y. Lian, Y. Zhang, S.H. Xia, *Food Chem.*, 209 (2016) 286-292.
7. A. Kussak, B. Andersson, K. Andersson, *J. Chromatogr. B*, 672 (1995) 253-259.
8. Y.R. Zhao, J.X. Huang, L.Y. Ma, F.H. Wang, *Food Chem.*, 221 (2017) 11-17.
9. S. Stefanovic, D. Spiric, R. Petronijevic, J.N. Trailovic, D. Milicevic, D. Nikolic, S. Jankovic, *Procedia Food Sci.*, 5 (2015) 270-273.
10. L.Z. Wang, Z. Wang, W.W. Gao, J. Chen, M.H. Yang, Y.F. Kuang, L. Huang, S.L. Chen, *Food Chem.*, 138 (2013) 1048-1054.
11. B.F. Huang, Z. Han, Z.X. Cai, Y.J. Wu, Y.P. Ren, *Anal. Chim. Acta*, 662 (2010) 62-68.
12. Q.H. He, Y. Xu, D. Wang, M. Kang, Z.B. Huang, Y.P. Li, *Food Chem.*, 134 (2012) 507-512.
13. Z.J. Li, Z.Y. Wang, X.L. Sun, Y.J. Fang, P.P. Chen, *Talanta*, 80 (2010) 1632-1637.
14. A. Gevaerd, C.E. Banks, M.F. Bergamini, L.H. Marcolino-Junior, *Sens. Actuators, B*, 307 (2020) 127547.
15. M.H. Banitaba, S.S. Davarani, A. Mehdinia, *Anal. Biochem.*, 411 (2011) 218-222.
16. X.L. Chen, G.M. Yang, S.P. Feng, L. Shi, Z.L. Huang, H.B. Pan, W. Liu, *Appl. Surf. Sci.*, 402 (2017) 232-244.
17. X.Q. Li, L.S. Wang, Q. Wu, Z.C. Chen, X.F. Lin, *J. Electroanal. Chem.*, 735 (2014) 19-23.
18. F.Y. Kong, L. Yao, R.F. Li, H.Y. Li, Z.X. Wang, W.X. Lv, W. Wang, *J. Alloys Compd.*, 797 (2019)

413-420.

19. Y.P. Liu, Z.X. Chang, L. Yao, S. Yan, J.J. Lin, J. Chen, J. Lian, H.L. Lin, S. Han, *J. Electroanal. Chem.*, 847 (2019) 113111.
20. S.N. Wang, S. Liu, J.Y. Zhang, Y. Cao, *Talanta*, 198 (2019) 501-509.
21. Y.R. Sun, C.Y. Du, M.C. An, L. Du, Q. Tan, C.T. Liu, Y.Z. Gao, G.P. Yin, *J. Power Sources*, 300 (2015) 245-253.
22. S.A. Wohlgemuth, R.J. White, M.G. Willinger, M.M. Titirici, M. Antonietti, *Green Chem.*, 14 (2012) 1515-1523.
23. S. Lin, D.H.K. Reddy, J.K. Bediako, M.H. Song, W. Wei, J.A. Kim, Y.S. Yun, *J. Mater. Chem. A*, 5 (2017) 13557-13564.
24. M. Yamada, M.R. Gandhi, Y. Kondo, F. Hamada, *Supramol. Chem.*, 26 (2014) 620-630.
25. Y.T. Qu, C. Li, L. Wang, Y.Z. Gao, J.C. Rao, G.P. Yin, *Int. J. Hydrogen Energy*, 41 (2016) 14036-14046.

© 2020 The Authors. Published by ESG ([www.electrochemsci.org](http://www.electrochemsci.org)). This article is an open access article distributed under the terms and conditions of the Creative Commons Attribution license (<http://creativecommons.org/licenses/by/4.0/>).